Biogeosciences Discuss., 9, 10019–10056, 2012
www.biogeosciences-discuss.net/9/10019/2012/
doi:10.5194/bgd-9-10019-2012

Biogeosciences Discussions

Nitrous oxide dynamics in low oxygen regions of the Pacific: insights from the MEMENTO database

L. M. Zamora[1], A. Oschlies[1], H. W. Bange[1], J. D. Craig[1], K. B. Huebert[2], A. Kock[1], and C. R. Löscher[3]

[1]GEOMAR | Helmholtz-Zentrum für Ozeanforschung Kiel, Düsternbrooker Weg 20, 24105 Kiel, Germany
[2]University of Hamburg Institute for Hydrobiology and Fisheries Science, Olbersweg 24, 22767 Hamburg, Germany
[3]Institut für Allgemeine Mikrobiologie, Christian-Albrechts-Universität zu Kiel, Am Botanischen Garten 1–9, 24118 Kiel, Germany

Received: 13 July 2012 – Accepted: 20 July 2012 – Published: 1 August 2012

Correspondence to: L. M. Zamora (lzamora@geomar.de)

Published by Copernicus Publications on behalf of the European Geosciences Union.

Abstract

The Eastern Tropical Pacific (ETP) is believed to be one of the largest marine sources of the greenhouse gas nitrous oxide (N_2O). Future N_2O emissions from the ETP are highly uncertain because oxygen minimum zones are expected to expand, affecting both regional production and consumption of N_2O. Here we assess three primary uncertainties in how N_2O may respond to changing O_2 levels: (1) the relationship between N_2O production and O_2 (is it linear or exponential at low O_2 concentrations?), (2) the cutoff point at which net N_2O production switches to net N_2O consumption (uncertainties in this parameterization can lead to differences in model ETP N_2O concentrations of more than 20 %), and (3) the rate of net N_2O consumption at low O_2. Based on the MEMENTO database, which is the largest N_2O dataset currently available, we find that N_2O production in the ETP increases linearly rather than exponentially with decreasing O_2. Additionally, net N_2O consumption switches to net N_2O production at $\sim 10\,\mu M$ O_2, a value in line with recent studies that suggest consumption occurs on a larger scale than previously thought. N_2O consumption is on the order of 0.129 mmol $N_2O\ m^{-3}\ yr^{-1}$ in the Peru–Chile Undercurrent. Based on these findings, it appears that recent studies substantially overestimated N_2O production in the ETP. In light of expected deoxygenation, future N_2O production is still uncertain, but due to higher-than-expected consumption levels, it is possible that N_2O concentrations may decrease rather than increase as oxygen minimum zones expand.

1 Introduction

The greenhouse gas nitrous oxide (N_2O) is produced and consumed in low oxygen regions of the ocean such as the Eastern Tropical Pacific (ETP) (Naqvi et al., 2010). Because oxygen minimum zones are expected to expand under ongoing global warming (Stramma et al., 2008; Deutsch et al., 2011), future regional N_2O emissions from the ETP are likely to change, perhaps even drastically (Codispoti, 2010). However, the factors that control marine N_2O production and consumption respond non-linearly to environmental changes and are not yet well understood (e.g. Bange et al., 2010). Therefore, the magnitude, and even sign, of the N_2O response to ocean deoxygenation is highly uncertain.

In a simplified view, N_2O concentrations within the ETP may be viewed as determined by three main factors: N_2O production rates, N_2O consumption rates at low O_2, and the O_2 value at which net N_2O production switches to net N_2O consumption. Currently, all of these factors have large associated uncertainties. For example, laboratory studies are at odds on whether N_2O production from bacterial nitrification increases exponentially or linearly with decreasing O_2 at low O_2 (Goreau et al., 1980; Frame and Casciotti, 2010). An exponential vs. linear parameterization can make a large difference in a model of marine N_2O production. N_2O consumption rates are even less certain than N_2O production rates; laboratory and in situ data differ by more than three orders of magnitude (e.g. Castro-González and Farías, 2004, and Codispoti and Christensen, 1985). There is also conflicting information for the O_2 value at which net N_2O production switches to N_2O consumption, with estimates ranging from 1–20 µM O_2 (e.g. Farías et al., 2009, and Suntharalingam et al., 2000). It is also problematic that much of the data available on N_2O production and consumption rates are based on laboratory studies, which only assess specific organisms and conditions that are not necessarily representative of the open ocean. For example, *archaea* were only recently recognized as major contributors to nitrification (e.g. Beman et al., 2012) and marine N_2O production (Santoro et al., 2010; Löscher et al., 2012), and information on their N_2O production rates is still very limited. N_2O production rates from anammox (Kartal et al., 2007) and nitrifier denitrification (e.g. Charpentier et al., 2007) are also not well constrained.

The MEMENTO database, which is the largest and most recent collection of 100+ cruises in which N_2O data were sampled (Bange et al., 2009), provides the unique opportunity to re-evaluate net marine in situ N_2O production and consumption rates, thus complementing laboratory studies. Here we quantitatively investigate the dynamics of marine N_2O in the Eastern Tropical Pacific, one of the ocean's largest suboxic zones. We estimate subsurface N_2O production rates at low O_2 concentrations in order to determine whether rates increase exponentially as previously predicted. We also examine in situ N_2O consumption rates in the ETP and estimate the O_2 concentration at which net N_2O production switches to net N_2O consumption. Finally, we test the sensitivity of N_2O distributions simulated by a global ocean model to uncertainties in these values.

2 Methods

2.1 Model description

For the model sensitivity analyses, the University of Victoria Earth System Climate Model (UVic-ESCM) version 2.9 was used with modifications described in Keller et al. (2012). The UVic-ESCM has a resolution of 3.6° longitude by 1.8° latitude with 19 vertical levels. The atmosphere is treated as one layer with homogeneous concentrations of atmospheric CO_2, O_2, CFC-12 and N_2O. The UVic-ESCM was initialized with World Ocean Atlas 2009 temperature (Locarnini et al., 2010), salinity (Antonov et al., 2010), oxygen (Garcia et al., 2010b), as well as nitrate and phosphate data (Garcia et al., 2010a). Each experiment was spun up for 13 800 yr under preindustrial atmospheric and astronomical boundary conditions before historical conditions were implemented for year 1744 and onwards, including increasing atmospheric N_2O (Holland et al., 2005), CO_2, and CFC-12 concentrations (Bullister, 2011) up to the year 2008. Atmospheric CO_2 was anthropogenically forced after 1744 and atmospheric O_2 was held constant. The UVic-ESCM resolves seasonal cycles, but does not incorporate large-scale climatological events like the El Niño Southern Oscillation.

Within the ocean, N_2O production rate per O_2 molecule consumed (nmol µmol^{-1}) was parameterized as a linear function of O_2 concentration: 1.69×10^{-4}–$4.8\times10^{-7} * O_2$ (mol m^{-3}). If O_2 concentrations fell below a threshold value of 10 µmol, N_2O consumption began (either at 0.0127, 0.127, and 1.27 mmol m^{-3} yr^{-1}, see

BGD

9, 10019–10056, 2012

N_2O dynamics in Pacific low O_2 regions

L. M. Zamora et al.

Sect. 3.2). To measure sensitivity to the threshold value at which net N_2O production switches to net N_2O consumption, values of 1, 4, 10, and 15 µM O_2 were also tested (see Sect. 3.3). For these sensitivity analyses, N_2O consumption rate was assumed to be 0.129 mmol N_2O m^{-3} yr^{-1}. N_2O production and consumption were assumed to be independent of temperature or depth. See Sects. 3.1–3.4 for details on why these parameterizations were selected.

For improved accuracy of current velocities in the Peru–Chile Undercurrent (Sect. 3.3), we used a higher resolution version of the global ocean model (the Geophysical Fluid Dynamics Laboratory Modular Ocean Model 4, or MOM4) (Zamora et al., 2010). This version of the MOM4 model had a 1° longitude by 1° latitude resolution with 50 vertical layers.

2.2 Transit time distributions

In order to correctly estimate N_2O production rates, it is important to distinguish the relative fractions of N_2O formed by in situ (i.e. biological) processes and N_2O originating from air-sea gas exchange (from when the water mass was in contact with the atmosphere), which itself has displayed increasing N_2O concentrations since preindustrial times. In the past, salinity- and temperature-based solubility calculations were typically used: the excess N_2O remaining after accounting for air-sea gas exchange (i.e. the "biotic" N_2O fraction) was labeled ΔN_2O (e.g. Yoshinari, 1976). Recently, water mass age estimates have been incorporated in abiotic N_2O calculations in order to address both water mass mixing and increasing atmospheric N_2O concentrations over the past 150 yr (Freing et al., 2009).

Here, we account for historic increases in atmospheric N_2O using the transit time distribution (TTD) method described in Freing et al. (2009) and Waugh et al. (2003) (see the Appendix for a more detailed description of the TTD method as applied here). Similarly to Waugh et al. (2003), we assume that a water parcel is a mixture of water with various ages, and that the density distribution of these ages can be described

BGD
9, 10019–10056, 2012

using an Inverse Gaussian distribution of the form:

$$G(t) = \sqrt{\frac{\Gamma^3}{\pi 4 \Delta^2 t^3}} \exp\left(\frac{-\Gamma(t-\Gamma)^2}{4\Delta^2 t}\right) \quad (1)$$

where t is time since ventilation at the ocean surface and Γ (mean age) and Δ (width) are the first and second moments of the distribution.

As in Freing et al. (2009), we estimate N_2O_{eq} (the N_2O concentration derived from equilibrium with atmospheric N_2O when the water was last in contact with the atmosphere) as follows:

$$[N_20]_{eq}^{TTD}(t) = \int_0^\infty H_{T,S} X_{N_2O}(t-t')G(t')dt', \quad (2)$$

where $H_{T,S}$ is solubility (Weiss and Price, 1980) and X_{N_2O} is the atmospheric dry mole fraction of N_2O at the estimated time of ventilation. For water masses ventilated before 1750, we assumed that the X_{N_2O} concentration was 270 ppb (Denman et al., 2007). After 1750, atmospheric N_2O dry mole fractions were assumed to increase according to (Holland et al., 2005).

The TTD method cannot be tested with in situ observations since it is impossible to know the actual N_2O_{eq} values with certainty. Therefore, we tested the validity of the TTD method by comparing modeled N_2O_{eq} with estimated N_2O_{eq} with where atmospheric N_2O was estimated by three methods: (1) the current model year (which would correspond to sample date if this method were used for observational data, as in Elkins et al., 1978), (2) atmospheric N_2O as estimated by modeled pCFC-12 age (which was calculated by matching observed pCFC-12 concentrations to the historic pCFC-12 concentration that would arise given the salinity and temperature of that water mass using solubility calculations from Warner and Weiss, 1985), and (3) the TTD age based on modeled pCFC-12 ages. This test was done for the year 2000 of the UVic-ESCM simulation (described in Sect. 2.1). Results, shown in Fig. 1, indicate that the

TTD method works well in the modeled ETP, with only a 3 % error between the model actual and model TTD estimated N_2O_{eq} values, providing a modest improvement in the estimation of the biotic N_2O component in comparison to methods used previously, even when a conservative Δ/Γ ratio of 1 is used (Fig. 1). For more information on Δ/Γ ratios relevant to this region, see the Appendix.

Once N_2O_{eq} values were calculated, the "biotic" N_2O portion of the total N_2O signal (N_2O_{xs}) was calculated as the difference between in situ N_2O concentrations and N_2O_{eq} (Freing et al., 2009):

$$N_2O_{xs} = N_2O_{in\ situ} - N_2O_{eq} \quad (3)$$

The TTD method also enables the calculation of water mass mean ages, thereby allowing a more accurate estimate of the N_2O production rate (N_2OPR):

$$N_2OPR = \frac{N_2O_{xs}}{\Gamma} \quad (4)$$

where Γ is the TTD calculated mean age of the water sample and N_2OPR is the average production rate the water parcel has experienced since last contact with the atmosphere

2.3 MEMENTO observations

N_2O observations were obtained from the MEMENTO database (version as of September 2011, see Fig. 2) (Bange et al., 2009). The Pacific MEMENTO database included 10 subsurface datasets gathered between 1976–2009 (station locations are shown in Fig. 2). Most of these N_2O datasets have been comprehensively described previously (Cohen and Gordon, 1978; Pierotti and Rasmussen, 1980; Friederich et al., 1992; Dore and Karl, 1996; Dore et al., 1998; Popp et al., 2002; Nevison et al., 2003; Charpentier et al., 2007; Farías et al., 2007; Ryabenko et al., 2012), with the exception of one cruise in the ETP (A. Kock and C. Löscher, unpublished data). N_2O values for all cruises were

BGD
9, 10019–10056, 2012

obtained by gas chromatography coupled with electron capture detectors. For most datasets, O_2 was determined by modified Winkler method (the exception being that of Charpentier et al., 2007, where O_2 was determined by CTD measurements calibrated with the Winkler method). Measurements of NO_2^-, NO_3^- and PO_4^{3-} were determined spectrophotometrically, and salinity/ temperature were obtained from CTD casts, with the exception of Pierotti and Rasmussen (1980) where temperature was measured by expendable bathythermograph and salinity was not measured.

In order to base our analysis on reliable data, we excluded some samples using the criteria discussed below. First, because gas exchange with the atmosphere and temperature-driven solubility changes create large uncertainties in the relative portion of N_2O with abiotic (N_2O_{eq}) and biotic (N_2O_{xs}) origins, all values from the upper 150 m were excluded. Second, we excluded all data with TTD mean age of ≤15 yr, since the oldest TTD mean age for which a negative N_2O_{xs} value was found was at 15 yr, indicating that samples with ages younger than 15 yr still had N_2O_{xs} values that were too low to reliably distinguish from N_2O_{eq} values. Excluding the samples with TTD ages < 15 yr effectively also eliminated all samples with AOU values of < 18 µM and O_2 saturations of > 95 %, thus also excluding data where N_2O_{xs}/AOU ratios (used in Sect. 3.1) would have been highly skewed by low AOU values in the denominator. Note: in a similar analysis that did not apply TTD methods, Nevison et al. (2003) dealt with this problem by excluding all data where AOU was < 50 µM. Third, to ensure data quality for the TTD determinations, we also removed all data with quality flags and samples with CFC-12 concentrations below 0.01 pM (a typical detection limit for CFC-12), and when relevant, with tritium values below 0.08 TU. Because we only examined waters with detectable CFC-12 values, most of the data used here were located in the 150–2000 m depth range. This depth range includes the region containing highest N_2O values (Fig. 3).

For the analysis of N_2O production rates presented in Sect. 3.1, it was necessary to exclude some additional data in order to ensure that these samples were not impacted by denitrification-driven N_2O consumption. Thus, for these analyses only we excluded samples with $O_2 < 10\,\mu M$, which is the highest O_2 value where we believe N_2O consumption could begin (see Sect. 3.2). Based on recent data presented by Cornejo and Farías (2012), a cutoff point of $10\,\mu M$ O_2 is a slightly conservative value (their data indicate that N_2O consumption in the ETSP starts at $8\,\mu M$ O_2). Because mixing may spread the signal of waters affected by N_2O consumption into nearby waters, we additionally excluded all samples where nitrite (NO_2^-) concentrations were > 0.1 (i.e. above detection limits). Nitrite is an intermediate of denitrification, among other processes, and it is an indicator of likely N_2O consumption (Cornejo and Farías, 2012) in the region below the upper (primary) NO_2^- maximum (~ 150 m) (Cline and Richards, 1972; Cohen and Gordon, 1978). As we excluded samples in the upper 150 m, there is minimal impact of the upper NO_2^- maximum on our analysis.

2.4 Calculating N_2O consumption rates

The N_2O consumption rate is calculated using Eq. (5) based on the method used by Codispoti and Christensen (1985):

$$N_2O \text{ consumption rate } (\text{mmol}\,N_2O\,\text{m}^{-3}\,\text{yr}^{-1}) = \frac{\text{loss of } N_2O\ (\text{mmol}\,\text{m}^{-3})}{\text{residence time (yr)}} \quad (5)$$

To estimate net N_2O consumption rates while minimizing the effects of local variability, we examined a region over $\sim 100\,000\,\text{km}^2$ from $\sim 6°$ S to 16° S and between the 26.3 and 26.5 σ_θ density layer (Fig. 4c). This region, which is located along the Peru–Chile undercurrent (PCUC), was selected because altimeter (Strub et al., 1995; Pizarro et al., 2002) and current-meter data (Shaffer et al., 1995; Czeschel et al., 2011) indicate a predominantly unidirectional flow along the coast, allowing a comparison in water mass chemical changes along the direction of water mass flow. Additionally, denitrification-driven N_2O consumption is likely occurring in this region based on decreases in N_2O and N^* concentrations (N^* is the deviation in inorganic nutrients from Redfield ratios, or $(NO_3^- + NO_2^-) - 16^*PO_4^{3-}$), an increase in NO_2^- concentrations, and uniformly low oxygen concentrations (< 10 µM) (Fig. 4). Samples from this region were collected in February 1985 (Friederich et al., 1992) and in February 2009 (Kock and Löscher, unpublished data). N_2O loss is calculated based on the reduction in N_2O concentrations along the direction of water mass flow (Fig. 4c) and water residence time is calculated based on timescale of water mass flow from model flow velocities (see Sect. 3.2).

3 Results and discussion

3.1 Subsurface N_2O production rates

The MEMENTO data show a slight linear increase in the N_2O_{xs}/AOU ratio (Fig. 5) with decreasing oxygen (note that expected spurious relationships between N_2O_{xs}/AOU and O_2, plotted in Fig. 5, have been ruled out as the cause for the observed pattern). Based on Fig. 5, for O_2 levels above 10 µM, observed subsurface N_2O_{xs}/AOU ratios (in nmol N_2O/µmol O_2) can be described by a linear relationship equaling 0.169–0.000243*O_2 (µM), with a median ratio of 0.131. Observed N_2O_{xs} results from the average N_2O production as the water mass transitioned from saturated O_2 to observed O_2. Therefore, the relationship between N_2O production and O_2 consumption corresponds to the relationship between observed N_2O_{xs} and the mean AOU during this transition. In this case the relationship is linear, and so mean AOU is equal to $(AOU_{observed} + AOU_{initial})/2 = (AOU + 0)/2 = 0.5\,AOU$. Thus, N_2O production derived from N_2O_{xs}/AOU ratios is best described by a slope of two times the observed slope with respect to O_2 (in this case, 0.00048 nmol N_2O/ µmol O_2).

In contrast to our findings, laboratory experiments conducted by Goreau et al. (1980) previously indicated that the yield of N_2O from bacterial nitrification increases exponentially with decreasing O_2, causing some later studies to parameterize N_2O production as exponentially related to O_2 concentrations (Suntharalingam et al., 2000, 2012; Nevison et al., 2003). However, more recent laboratory work indicates that bacterial

BGD
9, 10019–10056, 2012

nitrification N_2O production rates only exhibit exponential behavior under conditions rarely observed in the real ocean (i.e. cell densities > 10^6 cells ml^{-1} and < 0.5 % O_2 saturations) (Frame and Casciotti, 2010). Archaeal N_2O production rates also appear to increase as O_2 decreases (Löscher et al., 2012), although the archaeal N_2O production at very low O_2 (< 50 µM) has not been described to our knowledge. As an exponential vs. linear N_2O production parameterization would be expected to produce large differences in model N_2O concentrations, N_2O production at low O_2 concentrations has thus to date been a large uncertainty in models, especially near oxygen minimum zones.

Nevison et al. (2003), who examined the relationship between ΔN_2O/AOU ratios and O_2 concentrations using a dataset similar to the MEMENTO dataset, obtained similar distributions to that shown in Fig. 5. Thus, the use of ΔN_2O in Nevison et al. (2003) and our use of N_2O_{xs} as approximations for biotic N_2O did not appear to cause large differences in trends in biotic N_2O/AOU ratios. Although (Nevison et al., 2003) suggested that models use an exponential parameterization based on the Goreau et al. (1980) laboratory study, their data also showed no clear evidence for an exponential relationship between net N_2O production and O_2 concentrations, even in the O_2 ranges where N_2O exponential increases would be expected according to the Goreau et al. (1980) data.

For comparison in Fig. 5, we plot the expected exponential relationship between N_2O_{xs}/AOU ratio and O_2 based on Goreau et al. (1980) as defined in Eq. (6) in Nevison et al. (2003). Nevison et al. (2003) hypothesized that the lack of observed in situ exponential behavior might have been due to mixing with N_2O-depleted waters from OMZs. In addition to mixing, it is also possible that the lack of observed exponential behavior could be explained by a smaller than previously expected volume of water in which conditions exist where exponential behavior would be observable (as the data of Frame and Casciotti, 2010, seem to suggest). It is also worthwhile to emphasize that the Goreau et al. (1980) study was limited to bacterial nitrification. Therefore, it is possible that N_2O production from other sources, such as denitrification (e.g. Farías et al., 2009) or archaeal nitrification, is larger than previously thought and that these sources

BGD
9, 10019–10056, 2012

do not exponentially increase as O_2 declines. Independent of mechanism, it appears that the best description of net N_2O production in the ETP is a linear, not exponential, function of decreasing O_2.

Note that there is relatively high variability in the N_2O_{xs}/AOU ratios shown in Fig. 5. The MEMENTO median ratio of 0.131 nmol N_2O_{xs}/ µmol AOU falls within the range of other studies in the Eastern Pacific (0.08–0.22) based on linear slope calculations (Elkins et al., 1978; Cohen and Gordon, 1979; Cline et al., 1987; Butler et al., 1989; Nevison et al., 2003; Farías et al., 2007; Ryabenko et al., 2012). It is possible that some of the relatively high variability in N_2O produced per O_2 molecule consumed observed in Fig. 5 is due to mixing of water masses, the variable abundance of bacterial and archaeal nitrifiers (Beman et al., 2012), or composition and availability of organic matter (Nevison et al., 2003).

3.2 N_2O consumption rates

Here we focus on the Peru–Chile undercurrent (PCUC) region from ~6° S to 16° S and between the 26.3 and 26.5 σ_θ density layer (Fig. 4). As shown in Fig. 4, N_2O consumption is likely occurring in this region based on a decrease in N_2O concentrations of 0.0264–0.0407 mmol m^{-3}, a 13 µM decrease in N*, and a 5 µM increase in NO_2^- concentrations and uniformly low oxygen concentrations (< 10 µM) (see Sect. 3.3).

From Eq. (5), an assumed residence time of 0.32 yr (Table 1), and a N_2O loss of 0.0407 mmol m^{-3} (Table 1), we calculate an N_2O consumption rate of 0.129 mmol N_2O m^{-3} yr^{-1} within the 26.3 and 26.5 σ_θ density layer of focus. There is a relatively large uncertainty of one order of magnitude in the above rate due to uncertainties in water mass residence time (Table 1) as well as to uncertainties in flow of the PCUC caused by eddies (e.g. Czeschel et al., 2011 and Altabet et al., 2012).

The PCUC calculated N_2O consumption rate of 0.0129–1.29 mmol N_2O m^{-3} yr^{-1} is on the low-end of laboratory N_2O consumption rate measurements in ETP samples, which average from 1–1172 mmol m^{-3} yr^{-1} (Castro-González and Farías, 2004;

BGD
9, 10019–10056, 2012
N_2O dynamics in Pacific low O_2 regions
L. M. Zamora et al.

Title Page
Abstract | Introduction
Conclusions | References
Tables | Figures
◀| |▶
◀ ▶
Back | Close
Full Screen / Esc
Printer-friendly Version
Interactive Discussion

Farías et al., 2009). In contrast, the PCUC consumption rates are on the high-end of most geochemical estimates of net N_2O consumption rates, which range from 0.0005–0.012 mmol $N_2O\,m^{-3}\,yr^{-1}$ (Yamagishi et al., 2007) to 0.068 mmol $N_2O\,m^{-3}\,yr^{-1}$ (Codispoti and Christensen, 1985).

Some of the discrepancies between previously published laboratory and geochemical estimates of N_2O consumption may be due to local fluctuations in consumption rates; one laboratory study found that changes in O_2 concentrations and flux of organic matter could change N_2O consumption rates by up to one order of magnitude (Castro-González and Farías, 2004). As discussed, geochemical estimates may also suffer from uncertainties in water mass residence time and N_2O loss or perturbations induced by local eddies. However, it seems unlikely that these uncertainties alone would account for the 3+ orders of magnitude difference between laboratory and geochemical estimates in the literature. Part of the difference between laboratory measured and geochemically estimated N_2O consumption rates may also be caused by N_2O production occurring in the same waters in which N_2O consumption occurs, which would lower the net apparent consumption rates with respect to what would be observed in the laboratory.

Due to uncertainty in consumption rates, previous N_2O models have either not dealt with N_2O consumption at all (Nevison et al., 2003; Bianchi et al., 2012), or have arbitrarily assumed a linear drop in N_2O production down to zero after the switching point (Suntharalingam et al., 2000). Here, we used the UVic model to test the sensitivity of N_2O concentrations within the ETP to different values of N_2O consumption. Although there is a great deal of uncertainty in consumption values, we find that average modeled N_2O concentrations are relatively insensitive to uncertainties in consumption rates, affecting estimates by $< 10\,\%$ (Fig. 6b). Thus, the N_2O consumption rate estimate of 0.129 mmol $N_2O\,m^{-3}\,yr^{-1}$ provides an approximate value for consumption rates in the PCUC area, although obviously further work is necessary to better characterize marine N_2O consumption for the greater ETP region.

BGD
9, 10019–10056, 2012

3.3 The switch between net N_2O production and consumption

It is well known that as oxygen concentrations are reduced, eventually net N_2O production switches to net N_2O consumption, presumably due to denitrification. However, the exact O_2 concentration at which net N_2O consumption begins is not well defined. Models estimating N_2O production have previously used values of 1–4.5 µM O_2 (Suntharalingam et al., 2000; Nevison et al., 2003; Freing et al., 2012; Bianchi et al., 2012). However, literature estimates specific to the ETP place the switching point between 5–20 µM O_2 (Nevison et al., 2003; Farías et al., 2009; Cornejo and Farías, 2012; Ryabenko et al., 2012), indicating that the switching point may be higher than models have so far accounted for in this region.

The uncertainty in the point at which net N_2O consumption begins has important implications for modeling N_2O production in the ETP. Based on a sensitivity analysis, different literature values for the O_2 switching point yield up to a 22 % difference in expected ETP N_2O concentrations (Fig. 6). The large variability in expected N_2O concentrations is due to water volume. Based on mean corrected World Ocean Atlas 2005 data (Bianchi et al., 2012), the volume of water in the ETP that contains $\leq$ 5 µM O_2 is ~6 × smaller than that which contains $\leq$ 20 µM O_2. Thus, a switching point at 5 vs. 20 µM results in a disproportionately small volume of water in which N_2O can be consumed. Therefore, it is critical to correctly identify the O_2 concentration at which net N_2O production changes to net N_2O consumption in order to correctly predict N_2O concentrations in the ocean. This finding is in line with a recent study by Bianchi et al. (2012), which found that even without accounting for active N_2O consumption, global marine N_2O production was sensitive to the oxygen concentration at which net N_2O production stops.

Cornejo and Farías (2012) recently proposed using the development of subsurface nitrite (NO_2^-) as a proxy for N_2O consumption for the coastal Eastern Tropical South Pacific. NO_2^- is frequently associated with N_2O depletion; also, both NO_2^- reduction and N_2O production are inhibited at very low O_2 levels (Farías et al., 2007). As indicated

BGD
9, 10019–10056, 2012

in Fig. 7, subsurface NO_2^- accumulation in the ETP is also associated with low N^* and O_2, both indicators of denitrification. Based on NO_2^- concentrations > 0.75 µM, Cornejo and Farías (2012) identified the beginning of net N_2O consumption at 8 µM O_2 in the coastal Eastern Tropical South Pacific.

One problem with applying this approach to a broader scale is that NO_2^- may not be a good indicator of denitrification in all circumstances, even when the NO_2^- is accompanied by low N^* and low O_2 (Nicholls et al., 2007; Naqvi et al., 2010; Lam et al., 2011). Although NO_2^-, N_2O, low O_2, and low N^* can all be associated with water column denitrification, other processes such as anammox, sedimentary denitrification, and nitrification can affect the concentrations of these species as well. Additionally, accumulation of each can occur on different timescales, and each can also be passively transported.

Therefore, we use the MEMENTO database to test if NO_2^- is a good proxy for N_2O consumption over a larger region of the ETP than that described in Cornejo and Farías (2012) (the region in the MEMENTO database that includes NO_2^- data spans between 20° N–21° S and 70–110° W, Fig. 7). We find that when NO_2^- is low, N_2O production rates cover a range of values; conversely, when NO_2^- is above detection limits (~ 0.1 µM), N_2O production rates are almost always < 0.25 nmol kg^{-1} yr^{-1} (Fig. 7). Thus, NO_2^- appears to be a reliable proxy for N_2O consumption in the greater ETP. Similarly to Cornejo and Farías (2012), we find that NO_2^- accumulation begins when O_2 concentrations reach ~ 8–10 µM (Fig. 8). If an O_2 concentration of ~ 10 µM O_2 is a more realistic switching point than the 1–4 µM parameterized in previous models, these models may have vastly overestimated N_2O production in the ETP due to underestimating the volume involved in N_2O consumption.

Interestingly, others have reported lower points at which NO_2^- accumulates (e.g. 4 µM O_2 in the Eastern Tropical North Pacific (Cline and Richards, 1972, and 2.5 µM O_2 in the Arabian Sea, Morrison et al., 1998; Codispoti et al., 2001). The difference in the O_2 concentration at which NO_2^- accumulates and presumably N_2O consumption occurs

BGD
9, 10019–10056, 2012

indicates that there may be some fundamental difference between and within systems, perhaps due to the availability of organic matter or presence of specific nitrate reducing organisms in these regions.

3.4 Depth and temperature dependency of N_2O production

Multiple previous studies have suggested that there is a depth or temperature dependency of nitrification-produced N_2O (Elkins et al., 1978; Butler et al., 1989; Nevison et al., 2003; Freing et al., 2009). However, the temperature-sensitivity of nitrification rates is non-linear and may be masked or superseded by the dynamics of O_2 consumption (Barnard et al., 2005). While the focus of this manuscript is not on temperature or depth dependencies, we briefly note that the ETP MEMENTO data do not indicate a consistent temperature or depth dependence (Fig. 9).

4 Conclusions

Our findings support a growing body of work that indicates that N_2O consumption is occurring on a larger regional scale in the Pacific than initially expected. Previous models assume that net N_2O consumption begins at an O_2 concentration of 4 µM or lower. Our data indicate, based on TTD methods shown to robustly separate biotic and abiotic N_2O sources in the ETP, that N_2O consumption begins at ~10 µM O_2. Because ETP waters containing ≥ 10 µM O_2 have 3.5 × the volume of waters that contain ≥ 4 µM O_2, using a 4 vs. 10 µM O_2 switching point results in a 14 % overestimate in N_2O concentrations within the ETP. Thus, it is particularly important that models of N_2O production in expanding OMZs correctly identify the O_2 concentration at which net N_2O production switches to net consumption.

Our results also suggest that subsurface N_2O production at low O_2 concentrations remains nearly steady at about 0.00048 nmol N_2O produced per µmol O_2 consumed rather than increasing exponentially as previously expected. This finding, combined

BGD
9, 10019–10056, 2012

with a larger volume of water in which N_2O consumption occurs, points towards lower net regional N_2O production than estimated previously.

The dynamics of N_2O production at low O_2 concentrations are particularly important to constrain because oxygen minimum zones are thought likely to expand in the near future. To date, the response of N_2O production to expanding dexoxygenation is still highly uncertain due in large part to poorly constrained N_2O consumption rates-the consumption rates were uncertain enough that many previous studies have not accounted for N_2O consumption at all. We find that N_2O consumption rates in the Peru–Chile Undercurrent are on the order of 0.129 mmol N_2O m^{-3} yr^{-1} (± one order of magnitude). This value is several orders of magnitude lower than laboratory estimates of N_2O consumption rates but is consistent with other geochemical estimates for the ETP. However, it is uncertain how representative this value is of the overall ETP because N_2O consumption rates may vary due to local organic matter abundance and oxygen concentrations (Castro-González and Farías, 2004).

In order to improve estimates of N_2O production in the ETP, much more data on consumption rates is needed. If there is an increase in the volume of water in which net N_2O consumption occurs, it is possible that an expansion of the OMZs will cause average N_2O concentrations in the Pacific to decrease rather than increase.

Appendix A

Description of the transit time distribution (TTD) method

To determine the Δ/Γ ratio used in Eq. (1), we compared measured Pacific pCFC-12 age and tritium values with the TTD-derived values of pCFC-12 age and tritium associated with various Δ/Γ ratios (Fig. A1).

BGD
9, 10019–10056, 2012

The TTD-derived tracer concentrations were calculated as follows:

$$\text{CFC-12}^{\text{TTD}}_{r,t} = \int_0^{\infty} c_o(t-t')G(r,t')dt' \tag{A1}$$

$$^{3}\text{H}^{\text{TTD}}_{(r,t)} = \int_0^{\infty} c_o(t-t')e^{-\lambda t'}G(r,t')dt', \tag{A2}$$

where the TTD-derived tracer concentrations at a given point in space, r, and a given time, t, are a function of c_o (the input function of CFC-12 or ^3H at the sea surface) and, for ^3H, $e^{-\lambda t'}$ (the radioactive decay term of ^3H into ^3He), where λ is the decay rate of tritium into tritogenic He (0.05576 yr^{-1}) (Unterweger et al., 1980). The data shown in Fig. A1 are WOCE tritium data collected from 1989–1993 that were then normalized to tritium values expected in 1991.

The surface water pCFC-12 source function for the North Pacific was obtained using Northern Hemisphere atmospheric CFC-12 values from Walker et al. (2000), adapted up to 2008 using data from Bullister (2011) and using CFC-12 solubility coefficients from Warner and Weiss (1985). The surface water tritium source function for the North Pacific was obtained from Stark et al. (2004) using three latitudinal bands of surface tritium input for the tropics (0–20 °N), subtropics (20–40 °N), and subpolar regions (40–60 °N). Due to a paucity of data, accurate tritium inputs for the South Pacific were unavailable. Therefore, we focus our attention on data from the North Pacific, with ramifications discussed below. Both CFC-12 and tritium data are available from the World Ocean Circulation Experiment (WOCE) dataset (www.ewoce.org). As detailed in Sect. 2.2, the pCFC-12 age was calculated from CFC-12 concentrations based on atmospheric histories of CFC-12 and CFC-12 solubility.

Waters where upwelling is a dominant process are highly mixed. Thus we approximated the degree of upwelling-derived mixing using surface nitrate concentrations from the annual 1-degree World Ocean Atlas 2009 (Garcia et al., 2009). Samples with "low" and "high" upwelling-derived mixing were classified by having surface nitrate concentrations of $<1\,\mu M$ and $>1\,\mu M$, respectively (Fig. A2). Samples collected throughout

BGD
9, 10019–10056, 2012

the North Pacific indicate that a Δ/Γ ratio of 1 provides an accurate fit to observations in regions with high upwelling (such as the equatorial Pacific). In regions with low upwelling-derived mixing, a Δ/Γ ratio of 0.25 provides a better fit to the data (see Fig. A1).

Note that the data presented in Fig. A1 exclude Southern Hemisphere samples due to the lack of tritium data. For the MEMENTO data in the Southern Hemisphere, we assume that the relationship between upwelling-derived mixing and Δ/Γ ratios is similar in the North and South Pacific. This assumption is supported by previously published global model estimates of Δ and Γ (Peacock and Maltrud, 2005) that indicate that the patterns in Δ/Γ ratios are similar in the North and South Pacific.

Using a matrix containing individual Δ and Γ values and the corresponding TTD-derived pCFC-12 age, we determined each sample's Γ value by searching for the unique Γ value that corresponded to that sample's pCFC-12 age and Δ/Γ ratio. Because age tracer data were not available for the MEMENTO cruises, as in Freing et al. (2012) we used GLODAP gridded CFC-12 data (Key et al., 2004) for the calculation of Γ at the MEMENTO sites. Based on GLODAP gridded CFC-12 errors (Key et al., 2004) the median uncertainty in N_2O_{xs} and N_2OPR values resulting from extrapolating CFC-12 data to the collection sites was, respectively, 3 % and 31 %.

Acknowledgements. We thank R. Czeschel, A. Freing, J. Getzlaff, I. Montes, L. Stramma, T. Tanhua, and F. Wittke for help with this work. We would also like to thank P. Suntharalingam and C. Deutsch for helpful suggestions. Funding was provided by SOPRAN (FKZ 03F0611A) and SFB754.

The service charges for this open access publication have been covered by a Research Centre of the Helmholtz Association.

References

Altabet, M. A., Ryabenko, E., Stramma, L., Wallace, D. W. R., Frank, M., Grasse, P., and Lavik, G.: An eddy-stimulated hotspot for fixed nitrogen-loss from the Peru oxygen minimum zone, Biogeosciences Discuss., 9, 8013–8038, doi:10.5194/bgd-9-8013-2012, 2012.

Antonov, J. I., Sedov, D., Boyer, T. P., Locarnini R. A., Mishonov, A. V., and Garcia, H. E.: World Ocean Atlas 2009, Vol. 2: Salinity, NOAA Atlas NESDIS 69, US Government Printing Office, 2010.

Bange, H. W., Bell, T. G., Cornejo, M., Freing, A., Uher, G., Upstill-Goddard, R. C., and Zhang, G.: MEMENTO: a proposal to develop a database of marine nitrous oxide and methane measurements, Environ. Chem., 6, 195–197, doi:10.1071/EN09033, 2009.

Bange, H. W., Freing, A., Kock, A., and Löscher, C. R.: Marine pathways to nitrous oxide, in nitrous oxide and climate change, Marine pathways to nitrous oxide, in: Nitrous Oxide and Climate Change, edited by: Smith, K., Earthscan, New York, NY, USA, 36–62, 2010.

Barnard, R., Leadley, P. W., and Hungate, B. A.: Global change, nitrification, and denitrification: a review, Global Biogeochem. Cy., 19, GB1007, doi:10.1029/2004GB002282, 2005.

Beman, J. M., Popp, B. N., and Alford, S. E.: Quantification of ammonia oxidation rates and ammonia-oxidizing archaea and bacteria at high resolution in the Gulf of California and Eastern Tropical North Pacific Ocean, Limnol. Oceanogr., 57, 711–726, doi:10.4319/lo.2012.57.3.0711, 2012.

Bianchi, D., Dunne, J. P., Sarmiento, J. L., and Galbraith, E. D.: Data-based estimates of suboxia, denitrification, and N_2O production in the ocean and their sensitivities to dissolved O_2, Global Biogeochem. Cy., 26, GB2009, doi:10.1029/2011GB004209, 2012.

Bullister, J. L.: Atmospheric CFC-11, CFC-12, CFC-113, CCl_4, and SF_6 histories (1910–2011), Ocean CO_2 Carbon Dioxide Information Analysis Center, available at: http://cdiac.ornl.gov/oceans/new_atmCFC.html, last access: 23 May 2012.

Butler, J. H., Elkins, J. W., James, W., Thompson, T. M., Thayne, M., and Egan, K. B.: Tropospheric and dissolved N_2O of the West Pacific and East Indian Oceans during the El Niño southern oscillation event of 1987, J. Geophys. Res., 94, 14865–14877, 1989.

Castro-González, M. and Farías, L.: N_2O cycling at the core of the oxygen minimum zone off Northern Chile, Mar. Ecol.-Prog. Ser., 280, 1–11, doi:10.3354/meps280001, 2004.

BGD
9, 10019–10056, 2012

N_2O dynamics in Pacific low O_2 regions

L. M. Zamora et al.

Charpentier, J., Farias, L., Yoshida, N., Boontanon, N., and Raimbault, P.: Nitrous oxide distribution and its origin in the central and eastern South Pacific Subtropical Gyre, Biogeosciences, 4, 729–741, doi:10.5194/bg-4-729-2007, 2007.
Cline, J. D. and Richards, F. A.: Oxygen deficient conditions and nitrate reduction in the Eastern Tropical North Pacific Ocean, Limnol. Oceanogr., 17, 885–900, 1972.
Cline, J. D., Wisegarver, D. P., and Kelly-Hansen K.: Nitrous oxide and vertical mixing in the Equatorial Pacific during the 1982–1983 El Niño, Deep-Sea Res. Pt. I, 34, 857–873, doi:10.1016/0198-0149(87)90041-0, 1987.
Codispoti, L. A. and Christensen, J. P.: Nitrification, denitrification and nitrous oxide cycling in the Eastern Tropical South Pacific Ocean, Mar. Chem., 16, 277–300, doi:10.1016/0304-4203(85)90051-9, 1985.
Codispoti, L. A.: Interesting times for marine N_2O, Science, 327, 1339–1340, doi:10.1126/science.1184945, 2010.
Codispoti, L., Brandes, J. A., Christensen, J. P., Devol, A., Naqvi, S. W. A., Paerl, H. W., and Yoshinari, T.: The oceanic fixed nitrogen and nitrous oxide budgets: moving targets as we enter the anthropocene?, Sci. Mar., 65, 85–105, 2001.
Cohen, Y. and Gordon, L. I.: Nitrous oxide in the oxygen minimum of the Eastern Tropical North Pacific: evidence for its consumption during denitrification and possible mechanisms for its production, Deep-Sea Res., 25, 509–524, doi:10.1016/0146-6291(78)90640-9, 1978.
Cohen, Y., and Gordon, L. I.: Nitrous oxide production in the ocean, J. Geophys. Res., 84, 347–353, doi:10.1029/JC084iC01p00347, 1979.
Cornejo, M. and Farías, L.: Following the N_2O consumption at the Oxygen Minimum Zone in the eastern South Pacific, Biogeosciences Discuss., 9, 2691–2707, doi:10.5194/bgd-9-2691-2012, 2012.
Czeschel, R., Stramma, L., Schwarzkopf, F. U., Giese, B. S., Funk, A., and Karstensen, J.: Mid-depth circulation of the Eastern Tropical South Pacific and its link to the oxygen minimum zone, J. Geophys. Res., 116, C01015, doi:10.1029/2010JC006565, 2011.
Denman, K. L., Brasseur, G., Chidthaisong, A., Ciais, P., Cox, P. M., Dickenson, R. E., Hauglustaine, D., Heinze, C., Holland, E., Jacob, D., Lohmann, U., Ramachandran, S., da Silva Dias, P. L., Wofsy, S. C., and Zhang, X.: Couplings between changes in the climate system and biogeochemistry, in: Climate Change 2007: The Physical Science Basis. Contribution of Working Group I to the Forth Assessment Report of the Intergovernmental Panel on Climate

Change, edited by: Solomon, S., Qin, D., Manning, M., Chen, Z., Marquis, M., Averyt, K. B., Tignor, M., and Miller, H. L., Cambridge University Press, 2007.
Deutsch, C., Brix, H., Ito, T., Frenzel, H., and Thompson, L.: Climate-forced variability of ocean hypoxia, Science, 333, 336–339, doi:10.1126/science.1202422, 2011.
Dore, J. E. and Karl, D. M.: Nitrification in the euphotic zone as a source for nitrite, nitrate, and nitrous oxide at station ALOHA, Limn. Oceanogr., 41, 1619–1628, doi:10.4319/lo.1996.41.8.1619, 1996.
Dore, J. E., Popp, B. N., Karl, D. M., and Sansone, F. J.: A large source of atmospheric nitrous oxide from Subtropical North Pacific surface waters, Nature, 396, 63–66, doi:10.1038/23921, 1998.
Elkins, J. W., Wofsy, S. C., McElroy, M. B., Kolb, C. E., and Kaplan, W. A.: Aquatic sources and sinks for nitrous oxide, Nature, 275, 602–606, 1978.
Farías, L., Paulmier, A., and Gallegos, M.: Nitrous oxide and N-nutrient cycling in the oxygen minimum zone off Northern Chile, Deep-Sea Res. Pt. I, 54, 164–180, doi:10.1016/j.dsr.2006.11.003, 2007.
Farías, L., Castro-González, M., Cornejo, M., Charpentier, J., Faundez, J., Boontanon, N., and Yoshida, N.: Denitrification and nitrous oxide cycling within the upper oxycline of the Eastern Tropical South Pacific oxygen minimum zone, Limnol. Oceanogr., 54, 132–144, doi:10.4319/lo.2009.54.1.0132, 2009.
Frame, C. H. and Casciotti, K. L.: Biogeochemical controls and isotopic signatures of nitrous oxide production by a marine ammonia-oxidizing bacterium, Biogeosciences, 7, 2695–2709, doi:10.5194/bg-7-2695-2010, 2010.
Freing, A., Wallace, D. W. R., Tanhua, T., Walter, S., and Bange, H. W.: North Atlantic production of nitrous oxide in the context of changing atmospheric levels, Global Biogeochem. Cy., 23, GB4015, doi:10.1029/2009GB003472, 2009.
Freing, A., Wallace, D. W. R., and Bange, H. W.: Global oceanic production of nitrous oxide (N_2O), Philos. T. R. Soc. Lon. B, 367, 1245–1255, doi:10.1098/rstb.2011.0360, 2012.
Friederich, G. E., Codispoti, L., Spinrad, R. W., Packard, T. T., and Glover, H. E.: NITROP-85 Data Report, updated edition April 1992, in: Technical Report No. 59, Bigelow Laboratory for Ocean Sciences, 1992.
Garcia, H. E., Locarnini, R. A., Boyer, T. P., and Antonov, J. I.: World Ocean Atlas 2009, Vol. 4: Nutrients (Phosphate, Nitrate, Silicate), NOAA Atlas NESDIS 71, US Government Printing Office, 2010a.

Garcia, H. E., Locarnini, R. A., Boyer, T. P., Antonov, J. I., Baranova, O. K., Zweng, M. M., and Johnson, D. R.: World Ocean Atlas 2009, Vol. 3: Dissolved Oxygen, Apparent Oxygen Utilization, and Oxygen Saturation, NOAA Atlas NESDIS 70, US Government Printing Office, 2010b.

Goreau, T. J., Kaplan, W. A., Wofsy, S. C., McElroy, M. B., Valois, F. W., and Watson, S. W.: Production of NO_2^- and N_2O by nitrifying bacteria at reduced concentrations of oxygen, Appl. Environ. Microb., 40, 526–532, 1980.

Holland, E. A., Lee-Taylor, J., Nevison, C., and Sulzman, J.: Global N Cycle: Fluxes and N_2O Mixing Ratios Originating from Human Activity, Data Set, available at: http://www.daac.ornl.gov, Oak Ridge National Laboratory Distributed Active Archive Center, Oak Ridge, Tennessee, USA, doi:10.3334/ORNLDAAC/797, 2005.

Jenkins, W. J.: Tritium-helium dating in the Sargasso Sea: a measurement of oxygen utilization rates, Science, 196, 291–292, doi:10.1126/science.196.4287.291, 1977.

Kartal, B., Kuypers, M. M., Lavik, G., Schalk, J., Op den Camp, H. J. M., Jetten, M. S. M., and Strous, M.: Anammox bacteria disguised as denitrifiers: nitrate reduction to dinitrogen gas via nitrite and ammonium, Environ. Microbiol., 9, 635–642, doi:10.1111/j.1462-2920.2006.01183.x, 2007.

Keller, D. P., Oschlies, A., and Eby, M.: A new marine ecosystem model for the University of Victoria Earth system climate model, Geosci. Model Dev. Discuss., 5, 1135–1201, doi:10.5194/gmdd-5-1135-2012, 2012.

Key, R. M., Kozyr, A., Sabine, C. L., Lee, K., Wanninkhof, R., Bullister, J. L., Feely, R. A., Millero, F. J., Mordy, C., and Peng, T.-H.: A global ocean carbon climatology: results from global data analysis project (GLODAP), Global Biogeochem. Cy., 18, GB4031, doi:10.1029/2004GB002247, 2004.

Lam, P., Jensen, M. M., Kock, A., Lettmann, K. A., Plancherel, Y., Lavik, G., Bange, H. W., and Kuypers, M. M. M.: Origin and fate of the secondary nitrite maximum in the Arabian Sea, Biogeosciences, 8, 1565–1577, doi:10.5194/bg-8-1565-2011, 2011.

Locarnini, R. A., Mishonov, A. V., Antonov, J. I., Boyer, T. P., and Garcia, H. E.: World Ocean Atlas 2009, Vol. 1: Temperature, NOAA Atlas NESDIS 68, US Government Printing Office, 2010.

Löscher, C. R., Kock, A., Könneke, M., LaRoche, J., Bange, H. W., and Schmitz, R. A.: Production of oceanic nitrous oxide by ammonia-oxidizing archaea, Biogeosciences, 9, 2419–2429, doi:10.5194/bg-9-2419-2012, 2012.

BGD
9, 10019–10056, 2012

Montes, I., Colas, F., Capet, X., and Schneider, W.: On the pathways of the equatorial subsurface currents in the Eastern Equatorial Pacific and their contributions to the Peru–Chile Undercurrent, J. Geophys. Res., 115, C09003, doi:10.1029/2009JC005710, 2010.

Montes, I., Schneider, W., Colas, F., Blanke, B., and Echevin, V.: Subsurface connections in the Eastern Tropical Pacific during La Niña 1999–2001 and El Niño 2002–2003, J. Geophys. Res., 116, C12022, doi:10.1029/2011JC007624, 2011.

Morrison, J. M., Codispoti, L., Gaurin, S., Jones, B., Manghnani, V., and Zheng, Z.: Seasonal variation of hydrographic and nutrient fields during the US JGOFS Arabian Sea process study, Deep-Sea Res. Pt. II, 45, 1903–1931, 1998.

Naqvi, S. W. A., Bange, H. W., Farías, L., Monteiro, P. M. S., Scranton, M. I., and Zhang, J.: Marine hypoxia/anoxia as a source of CH_4 and N_2O, Biogeosciences, 7, 2159–2190, doi:10.5194/bg-7-2159-2010, 2010.

Nevison, C., Butler, J. H., and Elkins, J. W.: Global distribution of N_2O and the ΔN_2O-AOU yield in the subsurface ocean, Global Biogeochem. Cy., 17, 119, doi:10.1029/2003GB002068, 2003.

Nicholls, J. C., Davies, C. A., and Trimmer, M.: High-resolution profiles and nitrogen isotope tracing reveal a dominant source of nitrous oxide and multiple pathways of nitrogen gas formation in the Central Arabian Sea, Limnol. Oceanogr., 52, 156–168, 2007.

Peacock, S. and Maltrud, M.: Transit-time distributions in a global ocean model, J. Phys. Oceanogr., 36, 474–495, 2005.

Pierotti, D. and Rasmussen, R. A.: Nitrous oxide measurements in the Eastern Tropical Pacific Ocean, Tellus, 32, 56–72, 1980.

Pizarro, O., Shaffer, G., Dewitte, B., and Ramos, M.: Dynamics of seasonal and interannual variability of the Peru–Chile Undercurrent, Geophys. Res. Lett., 29, 1581, doi:10.1029/2002GL014790, 2002.

Popp, B. N., Westley, M. B., Toyoda, S., Miwa, T., Dore, J. E., Yoshida, N., Rust, T. M., Sansone, F. J., Russ, M. E., Ostrom, N. E., and Ostrom, P. H.: Nitrogen and oxygen isotopomeric constraints on the origins and sea-to-air flux of N_2O in the oligotrophic Subtropical North Pacific gyre, Global Biogeochem. Cy., 16, 1064, doi:10.1029/2001GB001806, 2002.

Ryabenko, E.: Nitrogen Isotopes in the Atlantic and Pacific Oxygen Minimum Zones, Ph.D. thesis, Christian-Albrechts-Universität zu Kiel, 2011.

Ryabenko, E., Kock, A., Bange, H. W., Altabet, M. A., and Wallace, D. W. R.: Contrasting biogeochemistry of nitrogen in the Atlantic and Pacific Oxygen Minimum Zones, Biogeosciences, 9, 203–215, doi:10.5194/bg-9-203-2012, 2012.
Santoro, A. E., Casciotti, K. L., and Francis, C. A.: Activity, abundance and diversity of nitrifying archaea and bacteria in the Central California Current, Environ. Microbiol., 12, 1989–2006, doi:10.1111/j.1462-2920.2010.02205.x, 2010.
Shaffer, G., Salinas, S., Pizarro, O., Vega, A., and Hormazabal, S.: Currents in the deep ocean off Chile (30° S), Deep-Sea Res. Pt. I, 42, 425–436, doi:10.1016/0967-0637(95)99823-6, 1995.
Stark S., Jenkins, W. J., and Doney, S. C.: Deposition and recirculation of tritium in the North Pacific Ocean, J. Geophys. Res., 109, C06009, doi:10.1029/2003JC002150, 2004.
Stramma, L., Johnson, G. C., Sprintall, J., and Mohrholz, V.: Expanding oxygen-minimum zones in the tropical oceans, Science, 320, 655–658, doi:10.1126/science.1153847, 2008.
Strub, P. T., Mesias, J. M., and James, C.: Altimeter observations of the Peru–Chile Countercurrent, Geophys. Res. Lett., 22, 211–214, doi:10.1029/94GL02807, 1995.
Suntharalingam, P., Sarmiento, J. L., and Toggweiler, J. R.: Global significance of nitrous-oxide production and transport from oceanic low-oxygen zones: a modeling study, Global Biogeochem. Cy., 14, 1353–1370, doi:10.1029/1999GB900100, 2000.
Suntharalingam, P., Buitenhuis, E., Quéré, C. L., Dentener, F., Nevison, C., Butler, J. H., Bange, H. W., and Forster, G.: Quantifying the impact of anthropogenic nitrogen deposition on oceanic nitrous oxide, Geophys. Res. Lett., 39, L07605, doi:10.1029/2011GL050778, 2012.
Unterweger, M. P., Coursey, B. M., Schima, F. J., Mann, W. B.: Preparation and calibration of the 1978 National Bureau of Standards tritiated water standards, Int. J. Appl. Radiat. Is., 31, 611–614, 1980.
Walker, S. J., Weiss, R. F., and Salameh, P. K.: Reconstructed histories of the annual mean atmospheric mole fractions for the halocarbons CFC-11 CFC-12, CFC-113, and carbon tetrachloride, J. Geophys. Res., 105, 14285–14296, doi:10.1029/1999JC900273, 2000.
Warner, M. J. and Weiss, R. F.: Solubilities of chlorofluorocarbons 11 and 12 in water and seawater, Deep-Sea Res., 32, 1485–1497, 1985.
Waugh, D. W., Hall, T. M., and Haine, T. W. N.: Relationships among tracer ages, J. Geophys. Res., 108, 3138, doi:10.1029/2002JC001325, 2003.

Weiss, R. F. and Price, B. A.: Nitrous oxide solubility in water and seawater, Mar. Chem., 8, 347–359, 1980.
Wyrtki, K.: The horizontal and vertical field of motion in the Peru Current, Bull. Scripps Inst. Oceanogr., 8, 313–346, 1963.
Yamagishi, H., Westley, M. B., Popp, B. N., Toyoda, S., Yoshida, N., Watanabe, S., Koba, K., and Yamanaka, Y.: Role of nitrification and denitrification on the nitrous oxide cycle in the Eastern Tropical North Pacific and Gulf of California, J. Geophys. Res., 112, G02015, doi:10.1029/2006JG000227, 2007.
Yoshinari, T.: Nitrous oxide in the sea, Mar. Chem., 4, 189–202, doi:10.1016/0304-4203(76)90007-4, 1976.
Zamora, L. M., Landolfi, A., Oschlies, A., Hansell, D. A., Dietze, H., and Dentener, F.: Atmospheric deposition of nutrients and excess N formation in the North Atlantic, Biogeosciences, 7, 777–793, doi:10.5194/bg-7-777-2010, 2010.

BGD
9, 10019–10056, 2012

Table 1. Estimated N_2O consumption rates within the Peru–Chile Undercurrent (PCUC) based on a range of estimated water mass residence times and on observed decreases N_2O concentrations for two separate cruises.

Data source[a]	Ventilation rate (Sv)	Volume (m^3)	Residence time (yr)	N_2O loss ($mmol\,m^{-3}$)	Estimated N_2O consumption rate ($mmol\,m^{-3}\,yr^{-1}$)
PCUC, between 26.3–26.5 σ_θ					
NITROP-85 cruise 1 (7.7–16° S, 1985) [1]					
Model-derived annual average (MOM4) [2]	0.11	1.1×10^{12}	0.31	0.0264	0.084
Model-derived annual average (ROMS) [3]	0.167	5.4×10^{12}	1.02	0.0264	0.026
M77/3 and M77/4 (6–14° S, 2009) [4]					
Model-derived annual average (MOM4) [2]	0.06	5.8×10^{11}	0.32	0.0407	0.129
Model-derived annual average (ROMS) [3]	0.13	4.1×10^{12}	1.01	0.0407	0.040
Observed instantaneous value, Feb. 2009 [5]	1.01	5.8×10^{11} [b]	0.02[b]	0.0407	2.035
Observed instantaneous value, Feb. 2009 [5]	1.01	4.1×10^{12} [c]	0.13[c]	0.0407	0.313
Entire PCUC					
Model-derived annual average (MOM4) [2]	4.0	–	–	–	–
Model-derived annual average (ROMS) [3]	1.8	–	–	–	–
Model-derived annual average (ROccam) [6]	3.9	–	–	–	–
Model-derived annual average (RSoda) [6]	4.9	–	–	–	–
Model-derived annual average (Uvic-ESCM) [7]	0.2	–	–	–	–
Observed instantaneous value [8]	2–4	–	–	–	–

[a] References are as follows: 1 – Friderich et al. (1992); 2 – Zamora et al. (2011); 3 – Montes et al. (2011) and I. Montes (personal communication, 2012); 4 – Kock and Löscher, unpublished data; 5 – Czeschel et al. (2011, Fig. 3f); 6 – Montes et al. (2010); 7 – this study, not used for calculation due to coarse resolution; 8 – Wyrtki (1963).
[b] Based on the MOM4-derived annual average volume.
[c] Based on the ROMS-derived annual average volume.

BGD
9, 10019–10056, 2012
N_2O dynamics in Pacific low O_2 regions
L. M. Zamora et al.

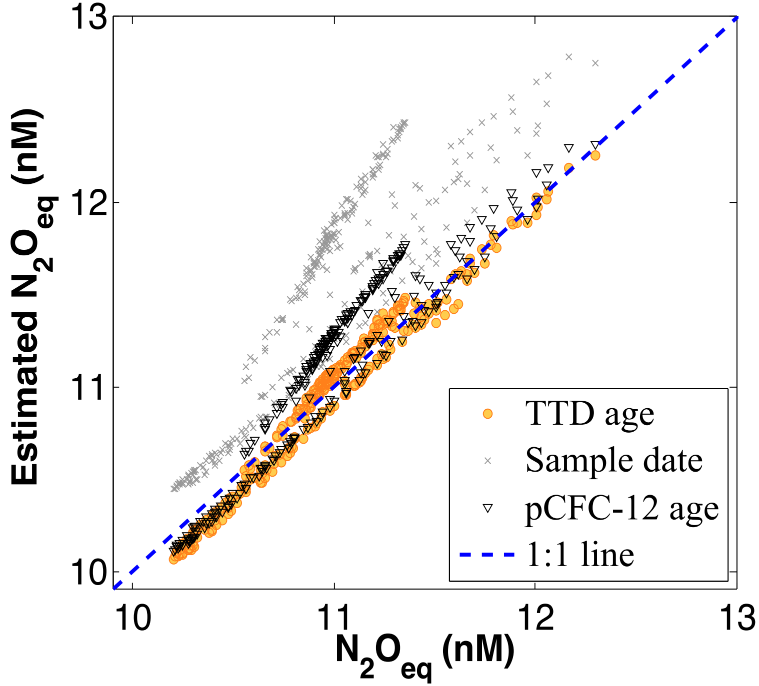

Fig. 1. The relationship between explicit model N_2O_{eq} values and N_2O_{eq} estimated from (1) the sampling date atmospheric N_2O values (in this case historical atmospheric N_2O variations are not accounted for)(gray crosses, $R^2 = 0.42$), (2) CFC-12 ages (black triangles, $R^2 = 0.85$), and (3) mean ages derived from the transit time distribution (TTD) method conservatively assuming "high" mixing (a Δ/Γ ratio of 1) at each site (orange circles, $R^2 = 0.96$). The R^2 values indicate how well each dataset describes the 1 : 1 line shown above (blue dashed line) using the sum of squares method. Data were obtained from the region between 10° N–23.5° S, 200–290° E, and within the 26.25–26.75 σ_Θ density layer.

BGD
9, 10019–10056, 2012

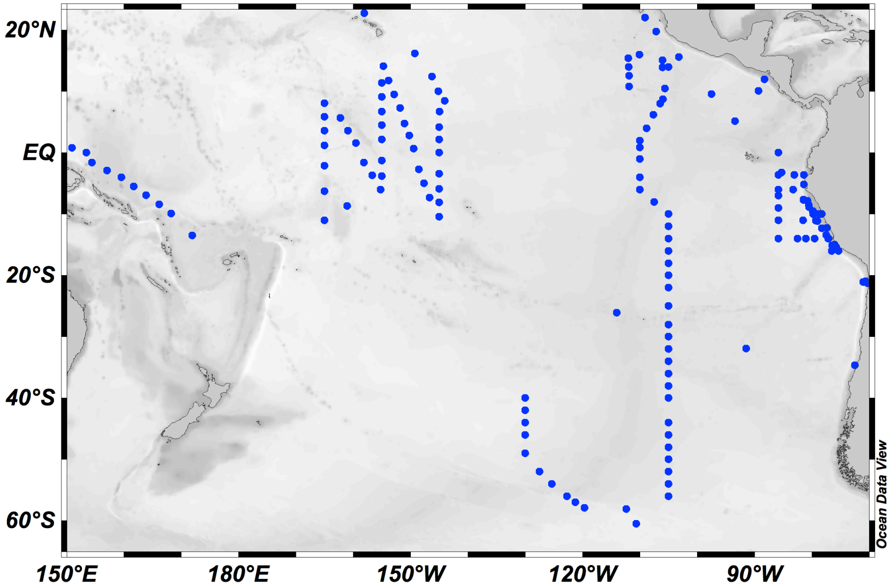

Fig. 2. Locations of Pacific sub-surface profiles contained in the MEMENTO dataset and used in this study.

BGD
9, 10019–10056, 2012

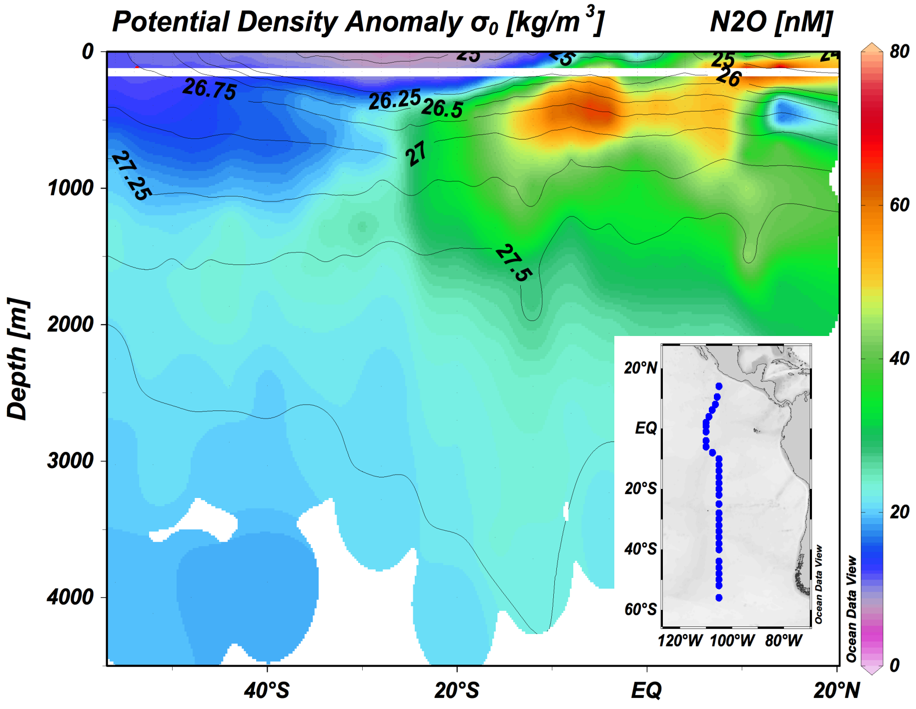

Fig. 3. Section of N_2O (nM) concentrations from the RITS89 cruise. In the Tropical and Subtropical Eastern Pacific, the bulk of N_2O is located in the upper 800 m. The white line indicates 150 m depth (above which data were excluded for reasons discussed in the text).

BGD
9, 10019–10056, 2012

N_2O dynamics in Pacific low O_2 regions

L. M. Zamora et al.

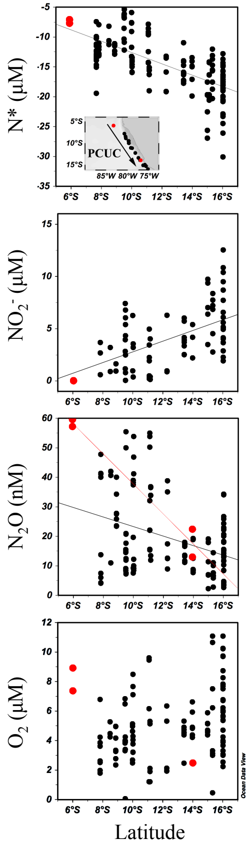

Fig. 4. Concentrations of NO_2^-, O_2, N_2O, and N* in the Peru-Chile Undercurrent (PCUC) in February 1985 (black) and February 2009 (red) between 26.3–26.5 σ_θ. Black and red lines are the least squares line for 1985 and 2009 data, respectively. The insert shows the station locations and the direction of flow for the PCUC.

BGD

9, 10019–10056, 2012

N_2O dynamics in Pacific low O_2 regions

L. M. Zamora et al.

Title Page
Abstract | Introduction
Conclusions | References
Tables | Figures
◀▌ | ▐▶
◀ | ▶
Back | Close
Full Screen / Esc
Printer-friendly Version
Interactive Discussion

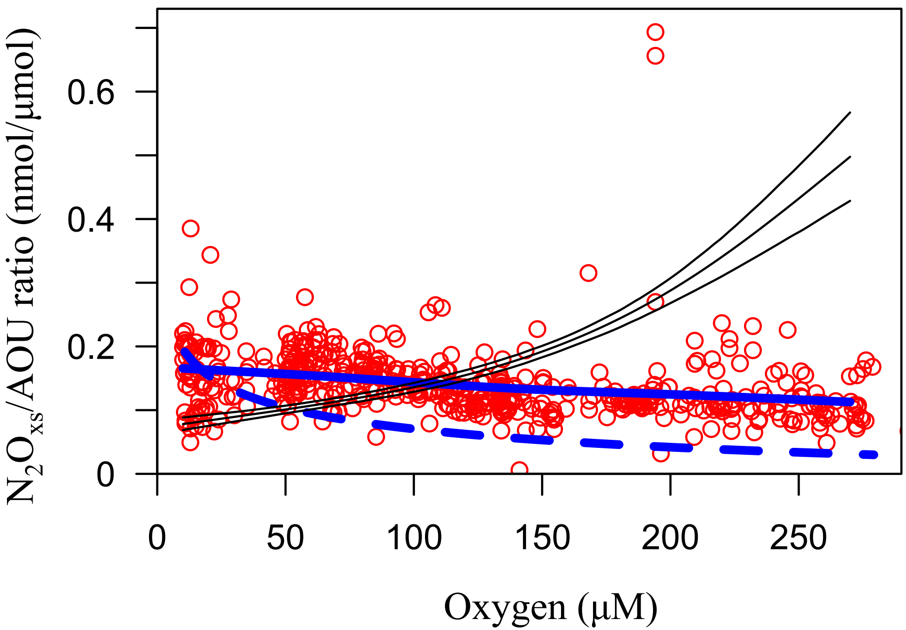

Fig. 5. N_2O_{xs}/AOU ratios vs. O_2 concentrations for MEMENTO profiles shown in Fig. 2. The thick, solid blue line is a spline (cubic smoothing) of the best fit for the data, with individual data shown in red. The dashed blue line indicates the expected cumulative production rate if production were to follow the Goreau et al. (1989) data as parameterized in Nevison et al. (2003) Eq. (6). Thin black lines are the spurious relationship (cubic smoothing splines for the median and 95 % confidence interval) that would be expected if the data were randomized. As spurious correlations have the opposite signal as the data, the relationship between N_2O_{xs}/AOU vs. O_2 observed is non-random.

BGD
9, 10019–10056, 2012

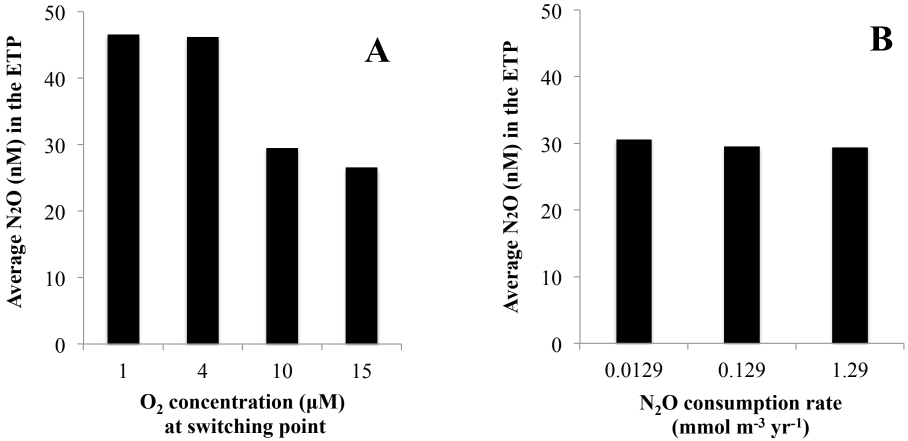

Fig. 6. Sensitivity of average modeled N_2O concentrations in the Eastern Tropical Pacific (ETP) between 80–150° W, 23.5° N-23.5° S, and 150–2000 m to **(a)** the O_2 concentration at which N_2O consumption begins (assuming an N_2O consumption rate of 0.129 mmol m^{-3} yr^{-1}), and **(b)** N_2O consumption rate (mmol m^{-3} yr^{-1}) (assuming a switching point of 10 mmol O_2 m^{-3}).

BGD
9, 10019–10056, 2012

Title Page
Abstract | Introduction
Conclusions | References
Tables | Figures
◀| |▶
◀ ▶
Back | Close
Full Screen / Esc
Printer-friendly Version
Interactive Discussion

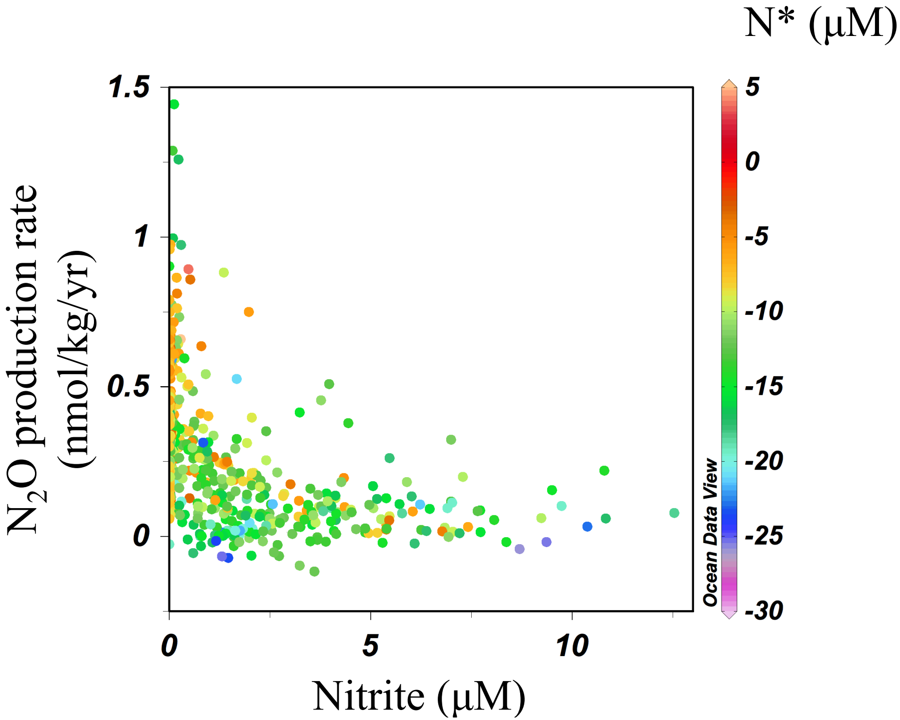

Fig. 7. ETP N_2O production rate (N_2OPR) vs. NO_2^- and N^* in the Eastern Tropical Pacific (ETP) (for the same region as in Fig. 2).

BGD
9, 10019–10056, 2012

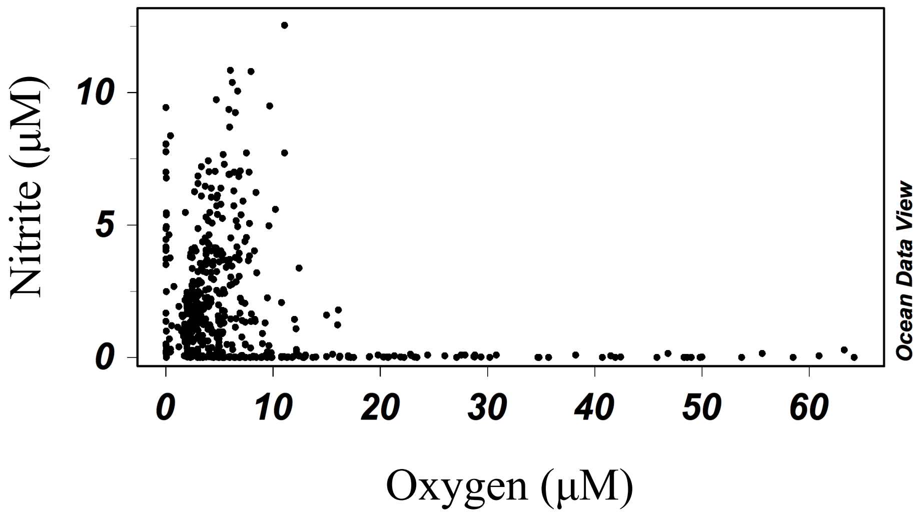

Fig. 8. NO_2^- (µM) and O_2 (µM) values in the ETP (for the same region as in Fig. 2) from depths > 150 m. NO_2^- accumulates at $O_2 < 10$ µM.

BGD
9, 10019–10056, 2012

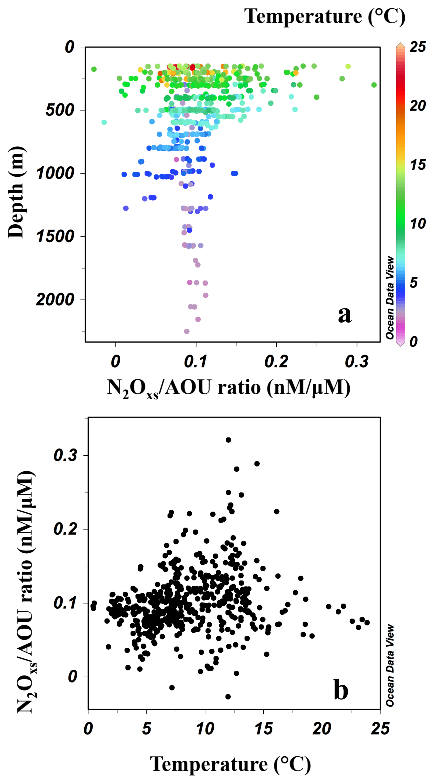

Fig. 9. O_2-corrected N_2O_{xs}/AOU ratios (nM/µM) vs. depth (m) and temperature (°C) for MEMENTO profiles shown in Fig. 2. O_2 dependency was corrected for by the linear relationship shown in Fig. 5, standardized to a fixed level of 276 µM O_2, the highest O_2 concentration observed in the selected data. Samples likely to be influenced by denitrification were excluded (see Sect. 2.3 for exclusion criteria). Note: in order to show detail, two outliers with high N_2O_{xs}/AOU ratios were excluded in the figures above.

BGD
9, 10019–10056, 2012

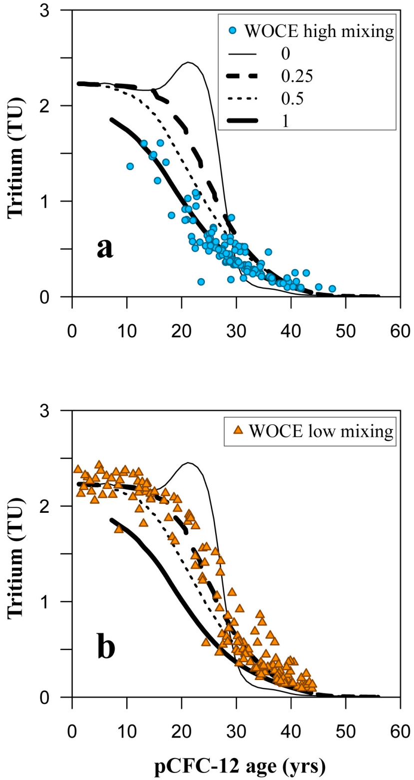

Fig. A1. The relationship between North Pacific pCFC-12 age and tritium concentrations normalized to year 1991 for observations and TTD-estimates based on equations A1 and A2. Observations (blue circles and yellow triangles) are from WOCE cruises PO4E (1989), P16C (1991), P17C (1991), P17N (1993), and P19C (1993). Observations are classified as "high mixing" (surface nitrate concentrations > 1 µM) and "low mixing" samples (surface nitrate concentrations < 1 µM) (see text for discussion on selection criteria). Samples with tracer concentrations below detection limits (i.e. CFC-12 concentrations < 0.01 pM; $^3H < 0.08$ TU) have been excluded. Black lines indicate the TTD-estimated pCFC-12 age and tritium values assuming a Γ/Δ ratio of 0, 0.25, 0.5, and 1 (thin solid, dashed, dotted, and thick solid lines, respectively). "High mixing" samples fit the ratio 1 line very well ($R^2 = 0.95$, total sum of square error technique) and "low mixing" samples fit the 0.25 ratio line well ($R^2 = 0.85$).

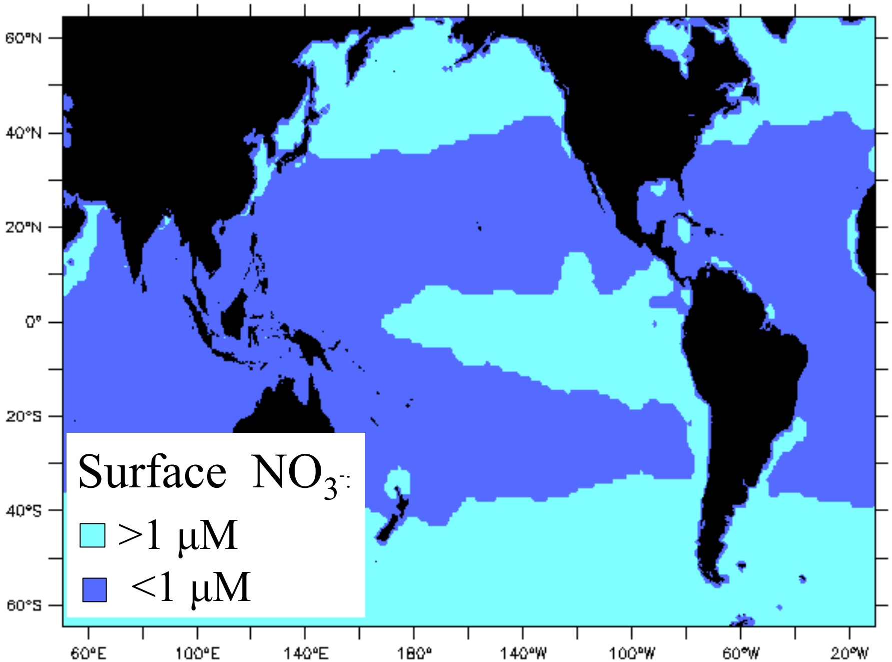

Fig. A2. Regions of the Pacific and surrounding regions where surface nitrate (NO_3^-) concentrations are above and below 1 µM. Based on the data in presented.

BGD
9, 10019–10056, 2012

N_2O dynamics in Pacific low O_2 regions

L. M. Zamora et al.

Title Page
Abstract | Introduction
Conclusions | References
Tables | Figures
◀| |▶
◀ ▶
Back | Close
Full Screen / Esc
Printer-friendly Version
Interactive Discussion